# Lawrence Berkeley National Laboratory

## Recent Work

### Title

Reevaluation of the p(2x2)S/Cu(001) Structure Using ARPEFS

### Permalink

https://escholarship.org/uc/item/5rt9c8jx

### Authors

Wittenau, A.E. Schach von
Hussain, Z.
Wang, L.Q.
et al.

### Publication Date

1991-11-01

eScholarship.org Powered by the California Digital Library
University of California

LBL-31501
Preprint

Lawrence Berkeley Laboratory
UNIVERSITY OF CALIFORNIA

Materials & Chemical
Sciences Division

Submitted to Physical Review B

# Reevaluation of the p(2x2)S/Cu(001) Structure Using ARPEFS

A.E. Schach von Wittenau, Z. Hussain, L.Q. Wang, Z.Q. Huang,
Z.G. Ji, and D.A. Shirley

November 1991

U. C. Lawrence Berkeley Laboratory
Library, Berkeley

FOR REFERENCE

Not to be taken from this room

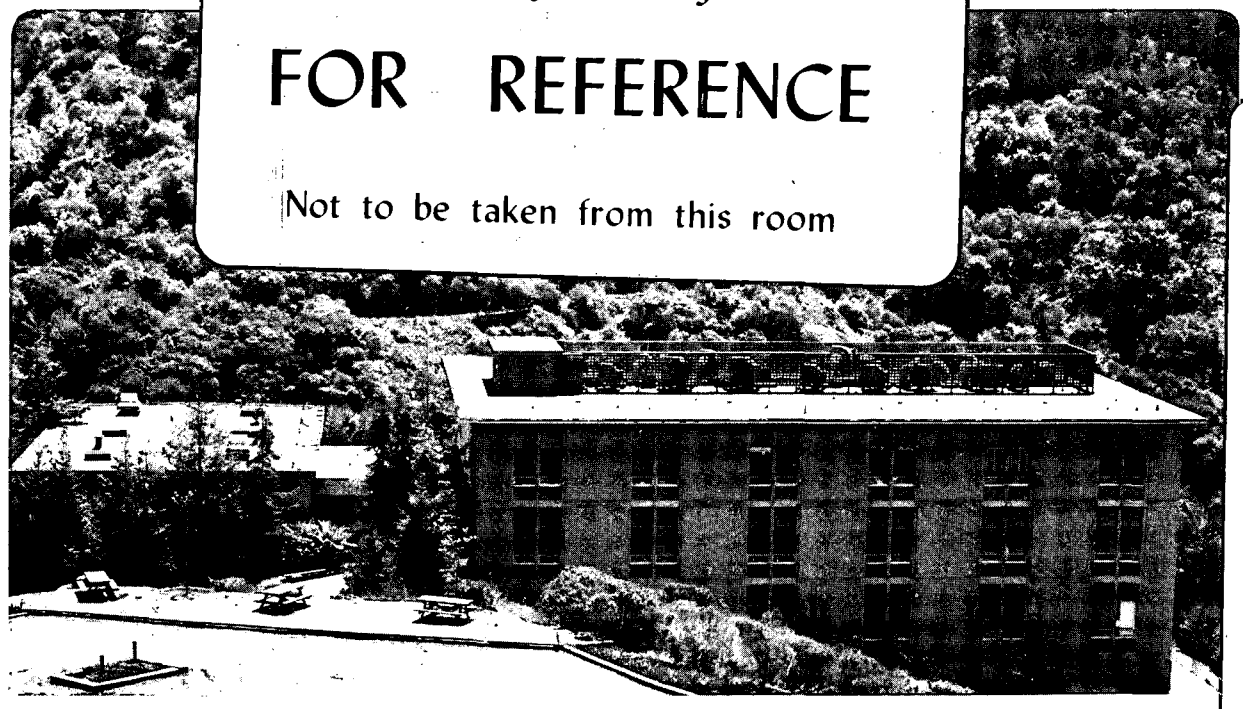

LBL-31501
Copy 1
Bldg. 50 Library.

Prepared for the U.S. Department of Energy under Contract Number DE-AC03-76SF00098

## DISCLAIMER

This document was prepared as an account of work sponsored by the United States Government. While this document is believed to contain correct information, neither the United States Government nor any agency thereof, nor the Regents of the University of California, nor any of their employees, makes any warranty, express or implied, or assumes any legal responsibility for the accuracy, completeness, or usefulness of any information, apparatus, product, or process disclosed, or represents that its use would not infringe privately owned rights. Reference herein to any specific commercial product, process, or service by its trade name, trademark, manufacturer, or otherwise, does not necessarily constitute or imply its endorsement, recommendation, or favoring by the United States Government or any agency thereof, or the Regents of the University of California. The views and opinions of authors expressed herein do not necessarily state or reflect those of the United States Government or any agency thereof or the Regents of the University of California.

LBL-31501

# Reevaluation of the p(2x2)S/Cu(001) Structure Using ARPEFS

A.E. Schach von Wittenau, Z. Hussain, L.Q. Wang,
Z.Q. Huang, Z.G. Ji, and D.A. Shirley

Department of Chemistry
University of California

and

Chemical Sciences Division
Lawrence Berkeley Laboratory
University of California
Berkeley, California 94720

November 1991

This work was supported by the Director, Office of Energy Research, Office of Basic Energy Sciences, Chemical Sciences Division, of the U.S. Department of Energy under Contract No. DE-AC03-76SF00098.

# Reevaluation of the p(2×2)S/Cu(001) Structure Using ARPEFS

A.E. Schach von Wittenau, Z. Hussain, L.Q. Wang,

Z.Q. Huang, Z.G. Ji*, and D.A. Shirley

*Department of Chemistry, University of California,*

*and*

*MS 2-300, Chemical Sciences Division, Lawrence Berkeley Laboratory, 1 Cyclotron Road, Berkeley CA 94720*

We have performed low-temperature (110 K – 160 K) Angle Resolved Photoemission Extended Fine Structure studies of p(2×2)S/Cu(001). Analysis based on Multiple Scattering Spherical Wave calculations indicates that S adsorbs into a four-fold hollow site 1.32 Å above the Cu surface, with near-surface reconstruction of the Cu layers in general similar to recent LEED and Medium Energy Ion Scattering results, removing an earlier discrepancy. The S-Cu bond length is determined to be 2.26 Å. The second-layer Cu(001) plane appears to be corrugated more than indicated by the other methods. Additional reconstruction may be present in this system.

## I. INTRODUCTION

The local atomic structure of p(2×2)S/Cu(001) has been studied by a variety of techniques, including Angle Resolved Photoemission Extended Fine Structure

(ARPEFS)[1], Surface Extended X-ray Absorption Fine Structure (SEXAFS)/X-Ray Standing Wave[2], Low Energy Electron Diffraction (LEED)[3–5], X-Ray Diffraction (XRD)[6], Electron Energy Loss Spectroscopy (EELS)[7], and Medium Energy Ion Scattering (MEIS)[8]. All of these studies agree that S occupies a fourfold hollow site. They differ, however, in the quantitative details of the adsorption geometry and on the effect of S adsorption upon the local structure of the Cu substrate. $D_{S1}$, the vertical distance between the S atoms and the first Cu layer, was found to be either $\sim$1.3 Å[5, 7, 8] or $\sim$1.4 Å[1, 2]. The Cu-S bond length was reported as having values between 2.23 Å and 2.31 Å.

Reconstruction of the near-surface layers was also found. Under p(2×2) symmetry, Cu atoms in the first layer, and all odd-numbered layers, may shift parallel to the surface (see Figures 2a and 2b). There are three inequivalent sites in the even-number layers, these are the 'covered', 'open', and 'anti-covered' sites. The 'covered' Cu atoms are directly below S adatoms. In the square pattern formed by the four S adatoms, the 'open' sites lie under the sides of this square. The 'anti-covered' sites are in the center of the square (see Figure 2b). Atoms in these inequivalent sites are allowed by symmetry to shift toward or away from the surface, but not laterally. The ARPEFS[1], LEED[5], and MEIS[8] results were analyzed for reconstruction in the two outermost Cu layers, subject to the above constraints. All three showed a lateral shift in the first layer Cu atoms: LEED[5] and MEIS[8] yielded an outward shift, away from the S adatom, of 0.02 Å and 0.03 Å, respectively, whereas ARPEFS[1] gave an inward shift of 0.05 Å. The conclusions about the second layer were equally striking: ARPEFS[1] gave a buckling of 0.12 Å, LEED[5] a buckling of 0.03 Å in the opposite sense, and MEIS[8] no buckling of the second layer. A summary of published p(2×2)S/Cu(001) structures, in our notation (Figure 2), is presented in Table I.

We performed new ARPEFS measurements, reported here, in an effort to resolve

differences between the previous ARPEFS[1] result and the recent LEED[5] study. Because of the small differences between the derived parameters in these two sets of results, (<0.1 Å for the nearest neighbor Cu atoms, <0.05 Å for more distant Cu atoms), high accuracy was essential. In this work we therefore made a significant departure from earlier ARPEFS methodology.

We sought to increase the magnitude of the ARPEFS oscillations by performing the measurements at low sample temperatures. Several $\chi(k)$ curves were taken at temperatures between 110 K and 160 K. Model MSSW calculations indicate that the structural differences between the published ARPEFS[1] and LEED[5] models affect $\chi(k)$ curves primarily at higher wavevector values. It is at these larger values of k, however, that photoelectron diffraction is most strongly attenuated by thermal motion of the substrate atoms. Experimental[9, 10] and theoretical[11] studies of bulk Cu indicate that cooling Cu to ~150 K would reduce $\sigma_j^2$, the mean-square relative displacement, for first shell atoms by at least 40%. Model calculations indicated that while at room temperature the two structures would yield qualitatively similar $\chi(k)$ curves for most of the trial experimental geometries investigated, cooling the Cu substrate to below ~150 K would increase the magnitude of the ARPEFS oscillations sufficiently to resolve differences between them.

## II. EXPERIMENTAL

A mechanically polished and chemically etched Cu(001) crystal was attached with tantalum strips to a tantalum sample plate, which was in turn mounted on a three-axis manipulator equipped with $LN_2$ cooling coils. The manipulator was installed in a UHV chamber equipped with an ion-sputtering gun, four-grid LEED/Auger optics and a moveable hemispherical analyzer[12, 13]. The crystal was cleaned by repeated cycles of $Ar^+$ sputtering (1 kV, $10^{-5}$ torr $Ar^+$) and annealing to 750 K until

sharp (1×1) LEED patterns were obtained and S, C, and O were not detectable by Auger spectroscopy. Ambient dosing of the clean room-temperature crystal with 60 L (120 sec., $5 \times 10^{-7}$ torr) $H_2S$, followed by annealing to 550 K, produced a sharp, stable p(2×2) overlayer. Temperatures were measured using a chromel-alumel thermocouple (referenced to room temperature) attached to the sample plate near the crystal.

Sulfur 1s ARPEFS data were taken using the double crystal monochromators on Beamline 3-3[14] at the Stanford Synchrotron Radiation Laboratory (SSRL) and on Beamline X-24A at the National Synchrotron Light Source[15]. Photoemission spectra were taken in the 50 eV - 550 eV (k=4.4 $Å^{-1}$ to 12 $Å^{-1}$) kinetic energy range using 2525 eV - 3025 eV photons. The analyzer was operated at 160 eV pass energy, giving an estimated overall energy resolution of ~2 eV. The chamber base pressure was $6 \times 10^{-11}$ torr to $3 \times 10^{-10}$ torr. During data collection the crystal was flashed periodically to 550 K to desorb any adsorbed contaminants.

Sulfur 1s photoemission spectra were taken in 0.07 $Å^{-1}$ to 0.1 $Å^{-1}$ increments over the energy range specified above. A total of 90 to 100 such spectra thus constitute a complete $\chi$(k) curve. Two normal emission $\chi$(E)curves were obtained, at sample temperatures of T = 110 K and 155 K. Two off-normal emission curves were also taken at 40° off normal (T = 140 K) in the [011] direction and at 50° off normal (T = 110 K) in the [011] direction, for a total of four curves.

## III. DISCUSSION

The ARPEFS data were reduced in the standard fashion[16]. Each individual S 1s photoemission spectrum was fitted as a sum of an empirical background function, a Voigt function, and a Gaussian broadened step function. The Lorentzian linewidth in the Voigt function was fixed at 0.8 eV. The means and Gaussian widths of the Voigt function and of the step function were constrained to be equal. Thus, each

individual photoemission spectrum was described by five parameters: the area of the Voigt function, the height of the step function, the mean and Gaussian width of the Voigt function, and the scale factor applied to the empirical background function. We then constructed an I(E) curve by plotting the area of the Voigt function against the Voigt mean energy, using the scaling factor of the empirical background to normalize each spectrum. In an EXAFS-like analysis we fitted a quadratic or cubic polynomial $I_0$ to these raw I(E) curves and formed $\chi$(E) curves using $I_t(E) = [1 + \chi(E)]\, I_0(E)$. The resulting $\chi$(E) curves are shown in Figure 3.

We calculated theoretical $\chi$(k) curves using the MSSW method described elsewhere[17]. Briefly, this model for ARPEFS calculates the interference between the primary photoelectron wave and the photoelectron waves scattered by atoms in the substrate. The method uses spherical waves and models the thermal vibration of the adsorbate and substrate atoms with a correlated Debye model. Effects of the finite angular acceptance of the analyzer and inelastic mean free path are also included.

There are three basic classes of parameters in any MSSW calculation. In order of decreasing importance they are the structural, experimental, and non-structural parameters. In fitting our data we assumed the same structural constraints used elsewhere[1, 5, 8]. Given the assumed $C_{4V}$ local symmetry of the p(2×2) overlayer, the atoms in the first Cu layer are constrained to be coplanar, but are allowed to shift radially with respect to the S adsorbate atom. The atoms in second layer are allowed to shift "vertically" (i.e., along the normal direction), but not horizontally. For simplicity and consistency with the earlier works[1, 5, 8] we assumed the atoms in the third and subsequent layers to be in their bulk positions. We thus have six structural parameters: $D_{S1}$ (the vertical distance between the S adatom and the first Cu layer), $D_{SC}$ (the vertical distance between the S adatom and the 'covered' Cu atom in the second layer), $D_{SO}$ (the vertical distance between the S adatom and the 'open'

Cu atom in the second layer), $D_{SA}$ (the vertical distance between the S adatom and the 'anti-covered' Cu atom in the second layer), $D_{S3}$ (the vertical distance between the S adatom and the third Cu layer), and the S-Cu bond length (see Figure 2). Note that any horizontal displacement of atoms in the first Cu layer is implicitly defined by $D_{S1}$ and the bond length.

There are five experimental parameters as well: the photoemission direction ($\hat{\theta}_e$,$\hat{\phi}_e$), the photon polarization ($\hat{\theta}_{h\nu}$,$\hat{\phi}_{h\nu}$), and the temperature of the sample during the ARPEFS experiment. In these experiments $\hat{\phi}_{h\nu}$ was always equal to $\hat{\phi}_e$ and in the (011) plane (Figure 1). For the off-normal measurements $\hat{\theta}_{h\nu} + \hat{\theta}_e$ was 90°. In the normal emission experiments $\hat{\theta}_{h\nu}$ was 50°. Because of the experimental difficulty of determining $\hat{\theta}_e$ and $\hat{\phi}_e$ (see Barton[18]) better than ±2°, these angles were treated as adjustable parameters in the fitting.

Finally there are such non-structural parameters as the Debye temperatures of the adsorbate and substrate, the angular acceptance of the analyzer, and the value of the inelastic mean free path $\lambda$. The bulk Debye temperature[19] for Cu was taken to be 320 K. The surface Debye[20] temperature for Cu was initially set at 184 K. The inelastic mean free path[21] was set at $\lambda = 0.75k$, where $\lambda$ is in units of Å and k is in units of $Å^{-1}$. The angular acceptance of the analyzer is taken to be 3° (half angle).

Phase shifts were calculated on a superposition potential[22] by using modified versions of programs by Loucks[23], with free-atom wavefunctions[24]. The phase shifts for sulfur were based on a hypothetical bcc lattice with lattice constant 2.26 Å. The lattice constant for Cu was taken to be 3.606 Å, the average of the 160 K and 110 K values[25, 26]. The exchange potential was modelled using the Slater X$\alpha$ approximation, with[27] $\alpha$=0.77.

To determine the values in Table II, we thus fitted each $\chi$(E) curve with eleven adjustable parameters (the six structural parameters, the two angles needed to de-

fine the experimental geometry (i.e. $\hat{\theta}_e$, $\hat{\phi}_e$), the isotropic adsorbate and substrate surface Debye temperatures, and the value of $V_0$ used in the deBroglie relation when converting from kinetic energy to wavevector).

## IV. PARAMETER DETERMINATION

We minimize the R-factor (see Appendix)

$$R_N = \frac{1}{N}\sum_{k_i}[\chi_T(k_i) - \chi_E(k_i)]^2 \qquad (1)$$

Here, $\chi_T(k_i)$ is theoretical value of $\chi(k_i)$ calculated using our MSSW model and $\chi_E(k_i)$ is the experimental value of $\chi(k_i)$. N is number of data points. We used a modified[30] simplex algorithm[31, 32] to minimize $R_N$.

The structural parameters for the vertices of the initial simplex were selected at random from a physically reasonable (typically $\pm 5\%$) range of values. $D_{S1}$ was taken to be in the range $1.25\text{Å} < D_{S1} < 1.45\text{Å}$. Fitting cycles were restarted from the 'best fit' of the previous cycle as a (useful) precaution against premature termination of the algorithm. Once 'convergence' had been achieved, a plot of R-factor versus parameter was made to determine error bars. Results of the process are shown in Table II.

Following the suggestions in reference 33, we performed the same analysis on the unweighted Fourier transforms of the $\chi(k)$ curves, that is, fitting the Fourier transforms of the $\chi(k)$ curves with the Fourier transforms of theoretical $\chi(k)$ curves. Since this should give the same result as fitting in k-space, this approach tests the uniqueness and reliability of the fitting process. Results of this fitting process are given in Table III. The fits are shown in Figures 4 – 7.

## V. ANALYSIS

### A. Normal Emission, 110 K and 155 K

The fits of these two normal emission $\chi$(E) curves in both k- and R-spaces are shown in Figure 4 and Figure 5. R-space and k-space fits generally converged to the same structure (see Tables II and III), the sole outlier being the value for $D_{S1}$ obtained by fitting the 110 K data in R-space. In the 155 K data we note that the amplitude of the oscillations in $\chi$(E) below 150 eV is underestimated by the theoretical curve: this problem is less severe for the 110 K curve. The regions around 200 eV and 350 eV are poorly described; the data show a smooth variation in $\chi$(E) here at both temperatures, whereas the theory curves all show double-peaked structures. Despite repeated efforts we have been unable to fit this region. Given that this reproducible discrepancy appears in curves representing independent data sets, we suspect that the surface reconstruction is actually more complicated than our present analysis assumes. Other "simple" adsorbate-substrate systems have been found to reconstruct substantially in recent years: S/Cu(001) may do so, too. However, by varying the positions of the nearest-neighbor Cu atoms around each S atom by small increments we were not able to improve the $\chi$(E) fits.

We note that for both the 110 K data and the 155 K data there is good agreement in peak positions between the data and theory, in the Fourier transforms, up to $R = 10 - 15$Å. Peak amplitudes are better matched for the 110 K data. We note an overall increase in the Fourier amplitudes for the 110 K data compared with the 155 K data (note the difference in scale between Figures 4c,d versus Figures 5c,d. For distances above 10–15 Å the agreement between experimental and theoretical Fourier peak positions declines rapidly. This is consistent with the misfits in $\chi$(E) noted above. The two experimental data sets, at 110 K and 155 K, are quite consistent with one another in both $\chi$(E) and its Fourier transform, through the regions where

theory cannot follow the data. We do not have a unique explanation for this behavior: several are possible. We are quite confidant that the main features of the local atomic environment of sulfur are understood. We are, however, also convinced that some subtlety of this system — reconstruction, a second phase, etc., — has eluded us and will require further study.

### B. 40° Off Normal Emission, 140 K

The fits were generally quite good. However, as with the normal emission data, we were unable to fit $\chi$(E) below approximately 100 eV (Figure 6). We also could not match the relative heights in the shoulders in the $\chi$(E) curve near the minimum at ~170 eV. There is good agreement of the peak positions in the Fourier transforms for both the k-space and R-space fits. We see in Figure 6d that improvement in agreement of the Fourier amplitudes below ~ 9 Å comes at the expense of peak position fits for the longer path length differences.

### C. 50° Off Normal Emission, 110 K

Again, the overall fits were quite good. The fitting of these data shows the same difficulties seen for the other three $\chi$(E) curves. The amplitude of the $\chi$(E) curve is poorly modelled below ~90 eV. The fitting in k-space otherwise yields good visual agreement and also gives a good agreement of the peak positions in the Fourier transforms. Fitting in R-space improves the agreement for the dominant peak, but, as was found with the 40° off-normal emission data, this comes at the expense of agreement for the other peaks. We note that this curve gives the most divergent results for $D_{S1}$: the fitting in k-space terminated at 1.37 Å, whereas in R-space the fit ended at 1.25 Å. The 50° off-normal emission curve is dominated by backscattering from one atom in the first Cu layer. While this gives a good estimate of the S-Cu

bond length, it does not give a reliable estimate for $D_{S1}$. Analysis of the path-length differences for scattering from the four Cu atoms nearest the S adatom indicates that this information would be contained as the shoulder on the low-R side of the main peak in the Fourier transform, and is obscured by the main peak.

### D. Overview

There were two main points of difference between the old ARPEFS[1] and the more recent LEED[5] and MEIS[8] structures. These were:

(a), the vertical distance between the S adatom and the first Cu layer, $D_{S1}$, and

(b), the degree and direction of the buckling in the second Cu layer.

Our values of $D_{S1}$ generally fell in the range 1.30 Å to 1.35 Å, with an average value of 1.32 Å. The new ARPEFS value is thus slightly larger than those from LEED [5] and MEIS[8], but within error limits.

In Figure 8 we show plots of the k-space fit residuals of the various $\chi(E)$ curves for $D_{SC}$, $D_{SO}$, and $D_{SA}$. There is a clear trend to smaller values as we go from substrate atom 'C' to substrate atom 'A'. While there is some scatter around the 'best' value, the trend is unmistakable. The fact that the R-factors for the fits in R-space yield the same trend indicates that ARPEFS at the present level of theory does unambiguously find this large a reconstruction. As an aside, we note that the normal emission curves give well defined and consistent results for the parameter $D_{SC}$. This is consistent with ARPEFS being sensitive to atoms lying along the electron emission direction. Both off-normal emission curves have large uncertainty in the position of atom 'C'; this is because the atom 'C' would have to scatter the photoelectron wave at an angle of 130° to 140° to appear in the off-normal emission curves. These angles correspond to an angular minimum in the scattering strength of Cu, hence the poor definition of $D_{SC}$ by the off normal curves. The photoemission paths to atoms 'O' and 'A' in the

second layer are somewhat out of alignment with the primary photoemission path to the detector; this and the increased pathlength differences yield less certainty in the determinations of $D_{SO}$ and $D_{SA}$.

By fitting parabolas to the minima of plots of R-factor versus each parameter, we extracted values for the parameters and their uncertainties. These are given in Tables II and III. Because of the scatter in the parameter determinations, and because in some cases the minima of these curves were poorly described by parabolas, we used these uncertainties as relative weights only (see Appendix) in determining the values given in Table IV.

Finally, we believe that the appearance of the fits shown in Figures 4–7 gives a fair impression of the potential of photoelectron diffraction only if we recall the demands that are being placed on our analysis. Our requirement that fits be made in both k-space and R-space is unique in placing stringent requirements on the data (which appear to do best), the theory, and the Fourier transform methodology. The $\chi$(E) amplitudes and the Fourier transform peak intensities are much less important than the frequencies in k-space or peak positions in R-space for determining structural parameters, but we have not weighted the latter parameters especially heavily in the R-factors. We have plotted the Fourier transforms out to 20 Å even though theory cannot be expected to follow experiment well above 10 Å, for various reasons. Finally, there may be additional reconstruction in this system which we have not been able to identify.

## VI. COMPARISON WITH PREVIOUS WORK

We note that the ARPEFS oscillations are enhanced at low temperature. In Figure 9 we show the normal emission curve from reference 1, taken at 300 K, and from the present study, taken at 110 K. The increase in the magnitude of oscillation

is evident. Given the internal consistency of the values in Table II, we decided to fit the older ARPEFS data from reference 1. We were able to obtain a good fit for the normal emission curve. Results of the k-space only fitting are shown in Table V, along with the value of the R-factor obtained using the structure given in reference 1. In Figure 10 we show the best fit. We note that use of the simplex algorithm instead of a hand search has yielded a better fit, and also, that the error bars are smaller for the normal emission curves taken at low temperature.

## VII. CONCLUSIONS

There is general agreement now about the first layer reconstruction of p(2×2)S/Cu(001). LEED, MEIS, and now ARPEFS all indicate that the S atom is 1.29 Å to 1.32 Å above the surface. Our value of 2.26 Å for the S-Cu bond length implies a 0.04 Å outward relaxation of the first layer Cu atoms, in agreement with LEED[5], XRD[6], and MEIS[8].

There is remains a strong quantitative difference regarding the second layer Cu atoms. Qualitatively, all three methods agree that, if there is a reconstruction of the second layer, it is in the direction $D_{SC} > D_{SO} > D_{SA}$. Quantitatively, however, ARPEFS indicates that the buckling is >0.08 Å, LEED yields 0.03 Å, and MEIS concludes that the buckling is 0.00 Å. This discrepancy is unresolved.

## VIII. ACKNOWLEDGEMENTS

This work was supported by the Director, Office of Energy Research, Office of Basic Energy Sciences, Chemical Sciences Division of the U.S. Department of Energy under Contract No. DE-AC03-76SF00098. It was performed at the Stanford Synchrotron Radiation Laboratory, which is supported by the Department of Energy's Office of Basic Energy Sciences, and at the National Synchrotron Light Source, which

is supported by the Department of Energy under Contract No. DE-AC02-76CH00016. We are deeply grateful to B. Karlin and D. Lindle for their assistance at NSLS. We also thank Prof. Gustafsson for sending us the MEIS results prior to publication. One of us (Z.H.) wishes to acknowledge the King Fahd University of Petroleum and Minerals for the grant of a sabbatical leave.

## APPENDIX A: ERROR ANALYSIS

The R-factor of Eq. 1 is chosen for its similarity to the standard $\chi^2$ statistic

$$\chi^2_\nu = \frac{1}{\nu}\sum_{k_i}\frac{[\chi_T(k_i) - \chi_E(k_i)]^2}{\sigma^2_{k_i}} \qquad \text{(A1)}$$

The definitions of the terms are the same as in Eq. 1, with the addition of $\nu$, the number of degrees of freedom ($\nu = N - 1$, where N is the the number of statistically independent points), and $\sigma(k_i)$, the noise estimate associated with point $k_i$. From considerations of the Nyquist sampling frequency we estimate, for Fourier filtered data, $N = \frac{1}{\pi}\Delta k \Delta R$, where $\Delta k = k_{max} - k_{min}$ is the range of the data and $\Delta R = R_{max} - R_{min}$ is the width of the R-space window[28, 33].

To minimize Eq. A1, we need an estimate for $\sigma(k_i)$. We may write[33] $\sigma^2_{total} = \sigma^2_{random} + \sigma^2_{systematic}$. We estimate our random noise level to be between 2% and 4%. We have found that adding a random 3% noise to a (necessarily smooth) theoretical $\chi(k)$ curve yields a curve that visually resembles a real $\chi(k)$ curve in roughness. This is the same estimate that we get by looking at the magnitude of the high (R > 18 Å) frequency components of our $\chi(k)$ curves. We have, unfortunately, no method of estimating the magnitude of any systematic errors in either the data reduction or in the theory. Were we to assume that $\sigma_{systematic} = 0$, we would have $\sigma_{total} \sim 0.03$. Since for a 'moderately good'[32] fit $\chi^2_\nu \sim 1$, this implies that our R-factor as defined in Eq. 1 should be quite close to $R_N = 0.0009$. As is shown

in Table II, this is not the case. In order to use the $\chi^2_\nu$ statistic we arbitrarily set $\sigma(k_i) = 1$ for all $k_i$ and proceed with the minimization, no longer having any independent evaluation of the goodness-of-fit of the result. Once the best $\chi^2_\nu$ (or $R_N$) has been obtained, we can estimate[34] the uncertainty $\sigma_{P_j}$ in any given parameter $P_j$ by

$$\sigma^2_{P_j} = 2\chi^2_{\nu_{best}} \times \left| \frac{\partial^2 \chi^2}{\partial P_j^2} \right|^{-1} \tag{A2}$$

where $\chi^2 = \nu\chi^2_\nu$ and $\chi^2_{\nu_{best}}$ is the lowest value of $\chi^2_\nu$ found. The partial derivatives in Eq. A2 are evaluated by fitting a parabola to the minimum of a graph of $R_N$ vs. $P_j$.

Once we have determined $P_j$ and $\sigma_j$, we estimate $\overline{P}$, the average value of P, and $\overline{\sigma}$, the uncertainty of $\overline{P}$, using

$$\frac{1}{\overline{\sigma}^2} = \sum_j \frac{1}{\sigma_j^2} \tag{A3}$$

and

$$\overline{P} = \overline{\sigma}^2 \sum_j \frac{P_j}{\sigma_j^2} \tag{A4}$$

Because of the scatter in the individual parameter determinations, we have chosen to regard the individual $\sigma_i$ as relative weights instead of absolute weights. While this does not affect the determination of $\overline{P}$, the uncertainty becomes

$$\overline{\sigma}'^2 = \frac{\overline{\sigma}^2}{N-1} \sum_j \frac{1}{\sigma_j^2} (P_j - \overline{P})^2 \tag{A5}$$

The uncertainties in Table IV are given by the larger of the values determined using Eqs. A3 or A5.

## REFERENCES


* Present Address: Department of Physics, Zhejiang University, Hangzhou, Zhejiang, China.

[1] C.C. Bahr, J.J. Barton, Z. Hussain, S.W. Robey, J.G. Tobin, and D.A. Shirley, Phys. Rev. B **35**, 3773 (1987).

[2] J.R. Patel, D.W. Berreman, F. Sette, P.H. Citrin, J.E. Rowe, P.L. Cowan, T. Jach, and B. Karlin, Phys. Rev. B, **40**, 1330 (1989).

[3] H.C. Zeng, R.N.S Sodhi, and K.A.R. Mitchell, Surf. Sci. **177**, 329 (1986).

[4] H.C. Zeng, R.A. MacFarlane, and K.A.R. Mitchell, Phys. Rev. B **39**, 8000 (1989).

[5] H.C. Zeng, R.A. MacFarlane, and K.A.R. Mitchell, Can. J. Phys. **68**, 353 (1990).

[6] E. Vlieg, I.K. Robinson, and R.McGrath, Phys. Rev. B **41**, 7896 (1990).

[7] Z.Q. Wu, M.L. Xu, Y. Chen, S.Y. Tong, M.H. Mohamed, and L.L Kesmodel, Phys. Rev. B **36**, 9329 (1987).

[8] Q.T. Jiang, P. Fenter, and T. Gustafsson, Phys. Rev. B **42**, 9291 (1990).

[9] E.A. Stern, D.E. Sayers, and F.W. Lytle, Phys. Rev. B **11**, 4836 (1975).

[10] R.B. Gregor and F.W. Lytle, Phys. Rev. B **20**, 4902 (1979).

[11] E. Sevillano, H. Meuth, and J.J. Rehr, Phys. Rev. B **20**, 4908 (1979).

[12] S.D. Kevan, Ph.D. thesis, University of California, Berkeley, (1980).

[13] S.D. Kevan and D.A. Shirley, Phys. Rev. B **22**, 542 (1980).

[14] Z. Hussain, E. Umbach, D.A. Shirley, J. Stoehr, and J. Feldhaus, Nucl. Instrum. Methods **195**, 115, (1982).

[15] P.L. Cowan, S. Brennan, R.D. Deslattes, A. Henins, T. Jach, and E.G. Kessler, Nucl. Instrum. Methods Phys. Res. Sect. A **246**, 154 (1986).

[16] L.J. Terminello, X.S. Zhang, Z.Q. Huang, S. Kim, A.E. Schach von Wittenau, K.T. Leung, and D.A. Shirley, Phys. Rev. B **38**, 3879 (1988).

[17] J.J. Barton, S.W. Robey, and D.A. Shirley, Phys. Rev. B **34**, 778 (1986).

[18] J.J. Barton, Ph.D. thesis, University of California, Berkeley, (1985).

[19] P.A. Flinn, G.M. McManus, and J.A. Rayne, Phys. Rev. B **123**, 809 (1961).

[20] D.L. Adams and U. Landman, Phys. Rev. B **15**, 3775 (1977).

[21] R. Trehan and C.S. Fadley, Phys. Rev. B **34**, 6784 (1986).

[22] L.F. Mattheiss, Phys. Rev. **113**, A134 (1964).

[23] T.L. Loucks, *Augmented Plane Wave Method*, (W.A. Benjamin) 1967.

[24] J.B. Mann, Los Alamos National Laboratory Report No. 3691 (1968).

[25] *Handbook of Chemistry and Physics*, (CRC Press) 1991.

[26] T.A. Hahn, J. Applied Physics **41**, 5096 (1970).

[27] J.F. Janak, A.R. Williams, and V. L. Moruzzi, Phys. Rev. B **6**, 4367 (1972).

[28] B.K. Teo, *EXAFS: Basic Principles and Data Analysis*, (Springer) 1986.

[29] S.W. Robey, J.J. Barton, C.C. Bahr, G. Liu, and D.A. Shirley, Phys. Rev. B **35**, 1108 (1987).

[30] J.M. Parkinson and D. Hutchinson, In *Numerical Methods for Non-linear Optimization*, (Academic Press) 1971.

[31] J.A. Nelder and R. Mead, Computer Journal **7** 308 (1965).

[32] W.H. Press, B.P. Flannery, S.A. Teukolsky, and W.T. Vetterling, *Numerical Recipes* (Cambridge University Press), 1989.

[33] F.W. Lytle, D.E. Sayers, and E.A. Stern, Physica B **158** 701, (1988).

[34] P.R. Bevington,*Data Reduction and Error Analysis for the Physical Sciences*, (McGraw-Hill) 1969.

## TABLES

TABLE I. Summary of structural parameters. Uncertainties in the last digit of each parameter, where given, are in parentheses.

| $D_{S1}$ | $D_{SC}$ | $D_{SO}$ | $D_{SA}$ | $D_{S3}$ | $D_{S-Cu}$ | $\Delta$ | Method |
|---|---|---|---|---|---|---|---|
| 1.42(2) | 3.04(2) | 3.07(6) | 3.16(5) | 4.97(6) | 2.26(1) | -0.05(2) | ARPEFS [1] |
| 1.28(3) | 3.12 | 3.11 | 3.09 | 4.94 | 2.23(6) | +0.02 | LEED [5] |
| 1.30 | 3.11 | 3.11 | 3.11 | 4.93 | 2.25 | +0.03 | MEIS [8] |
| 1.19(14) | - | - | - | - | - | +0.03(1) | XSW [6] |
| 1.40(4) | - | - | - | - | 2.31(2) | - | SEXAFS [2] |
| 1.30(5) | - | - | - | - | - | - | ELS [7] |

TABLE II. Results of k-Space Fitting.

| Parameter | Normal Emission | | Off Normal Emission | |
|---|---|---|---|---|
| | 110 K | 155 K | 140 K, 40° | 110 K, 50° |
| $D_{S1}$ | 1.31(2) | 1.32(1) | 1.34(1) | 1.37(3) |
| $D_{SC}$ | 3.19(1) | 3.17(1) | 3.17(3) | 3.22(8) |
| $D_{SO}$ | 3.11(2) | 3.13(2) | 3.19(2) | 3.12(2) |
| $D_{SA}$ | 3.07(3) | 3.09(2) | 3.08(3) | 3.05(2) |
| $D_{S3}$ | 4.89(2) | 4.91(2) | 4.92(4) | 4.89(3) |
| Bond | 2.25(2) | 2.27(2) | 2.27(1) | 2.27(1) |
| $\Delta$ | +0.02(2) | +0.04(3) | +0.03(1) | +0.01(3) |
| $V_o$ | 12.7 | 11.7 | 10.7 | 11.6 |

TABLE III. Results of R-Space Fitting

| Parameter | Normal Emission | | Off Normal Emission | |
|---|---|---|---|---|
| | 110 K | 155 K | 140 K, 40° | 110 K, 50° |
| $D_{S1}$ | 1.37(2) | 1.31(2) | 1.31(1) | 1.25(1) |
| $D_{SC}$ | 3.18(1) | 3.19(1) | 3.22(6) | 3.22(8) |
| $D_{SO}$ | 3.12(3) | 3.12(3) | 3.15(2) | 3.19(4) |
| $D_{SA}$ | 3.08(4) | 3.02(4) | 3.03(2) | 3.02(4) |
| $D_{S3}$ | 4.89(2) | 4.91(2) | 4.83(2) | 5.10(8) |
| Bond | 2.25(2) | 2.26(2) | 2.25(1) | 2.26(1) |
| $\Delta$ | -0.01(3) | +0.04(2) | +0.02(1) | +0.08(1) |
| $V_o$ | 12.6 | 11.2 | 12.5 | 11.6 |

TABLE IV. Average Value of Parameter

| Parameter | k Space Fitting | R Space Fitting | Assigned Value |
|---|---|---|---|
| $D_{S1}$ | 1.33(1) | 1.30(2) | 1.32(1) |
| $D_{SC}$ | 3.18(1) | 3.19(1) | 3.18(1) |
| $D_{SO}$ | 3.14(2) | 3.14(1) | 3.14(1) |
| $D_{SA}$ | 3.07(1) | 3.03(2) | 3.06(1) |
| $D_{S3}$ | 4.90(1) | 4.89(2) | 4.90(1) |
| Bond | 2.27(1) | 2.25(1) | 2.26(1) |
| $\Delta$ | +0.03(1) | +0.04(2) | +0.04(1) |

TABLE V. Results of k-Space Fitting of Normal Emission 300 K Data. The 'Old R-Factor' is based on the structure given in ref. [1]

| Parameter | 300 K Normal Emission |
|---|---|
| $D_{S1}$ | 1.31(2) |
| $D_{SC}$ | 3.18(2) |
| $D_{SO}$ | 3.07(3) |
| $D_{SA}$ | 3.05(4) |
| $D_{S3}$ | 4.94(3) |
| Bond | 2.24(3) |
| $\Delta$ | +0.00(4) |
| $V_o$ | 12.62 |
| R-factor | .0016 |
| Old R-factor | .0062 |
| N | 26 |

## FIGURES

FIG. 1. Diagram of the experimental geometry.

FIG. 2. Schematic of p(2×2)S/Cu(001), showing structure and label definitions.

(a) Top view, showing outward reconstruction of first layer Cu atoms.

(b) Side view, showing vertical relaxations of second layer Cu atoms.

FIG. 3. Raw $\chi$(E) Curves.

(a) Normal Emission (110 K).

(b) Normal Emission (155 K).

(c) 40° Off Normal Emission (140 K).

(d) 50° Off Normal Emission (110 K).

FIG. 4. Results of fitting the normal emission (110 K) data in k-space and R-space. The k-space curves are Fourier filtered at 1.4 Å < R < 14.4 Å.

(a) and (c): Comparison of data (dots) and theory (solid line) curves. Fit performed in k-space.

(b) and (d): Comparison of data (dots) and theory (solid line) curves. Fit performed in R-space.

FIG. 5. Results of fitting the normal emission (155 K) data in k-space and R-space. The k-space curves are Fourier filtered at 1.2 Å < R < 12.8 Å.

(a) and (c): Comparison of data (dots) and theory (solid line) curves. Fit performed in k-space.

(b) and (d): Comparison of data (dots) and theory (solid line) curves. Fit performed in R-space.

FIG. 6. Results of fitting the 40° off normal emission (140 K) data in k-space and R-space. The k-space curves are Fourier filtered at 2.1 Å < R < 15.4 Å.

(a) and (c): Comparison of data (dots) and theory (solid line) curves. Fit performed in k-space.

(b) and (d): Comparison of data (dots) and theory (solid line) curves. Fit performed in R-space.

FIG. 7. Results of fitting the 50° off normal emission (110 K) data in k-space and R-space. The k-space curves are Fourier filtered at 2.4 Å < R < 13.8 Å.

(a) and (c): Comparison of data (dots) and theory (solid line) curves. Fit performed in k-space.

(b) and (d): Comparison of data (dots) and theory (solid line) curves. Fit performed in R-space.

FIG. 8. Residuals vs. the vertical distances between the S adatom and the Cu atoms in the second layer, k-space fits only.

Panels:

Top: Residuals vs. $D_{SC}$

Middle: Residuals vs. $D_{SO}$

Bottom: Residuals vs. $D_{SA}$

The solid lines are cubic spline interpolations as guides to the eye. Note that the curves for the normal-emission data show well defined and reproducible minima for $D_{SC}$, whereas the off-normal data are quite insensitive to this parameter. The dashed line through the panels shows the positions of the assigned value of each parameter.

Symbols:

■ : Normal emission, 110 K data.

● : Normal emission, 155 K data.

○ : 40° Off normal emission, 140 K data.

□ : 50° Off normal emission, 110 K data.

FIG. 9. Comparison of Fourier filtered (2 Å< R < 11 Å) normal emission $\chi$(E) curves taken at 110 K (this work) and 300 K (ref [1]).

FIG. 10. Fit to 300 K normal emission data from ref [1].

Symbols:

Crosses: Best k-space fit.

Circles: Data.

Figure: 1: Experimental Geometry.

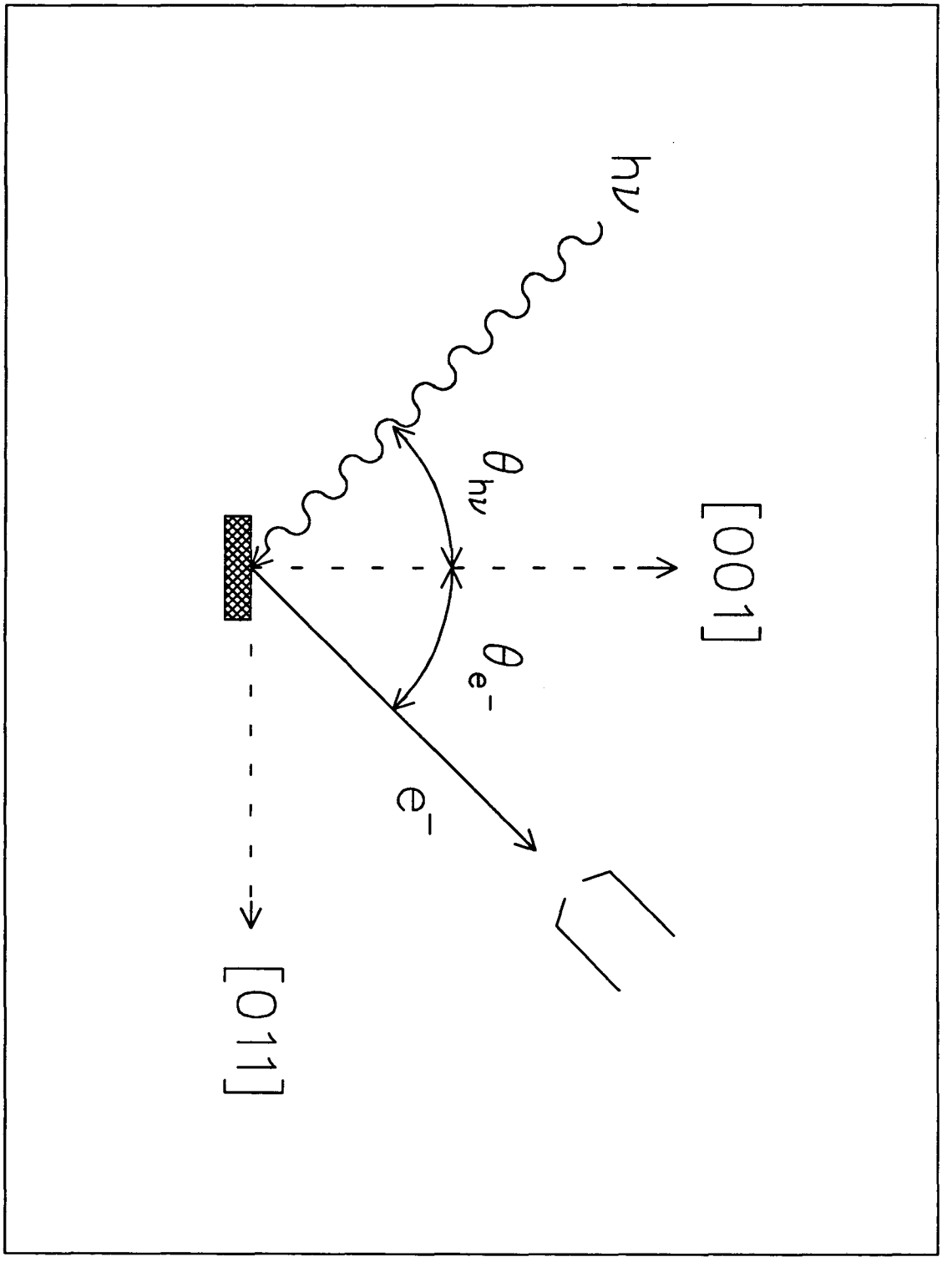

Figure: 2: p(2×2)S/Cu(001) Structure.

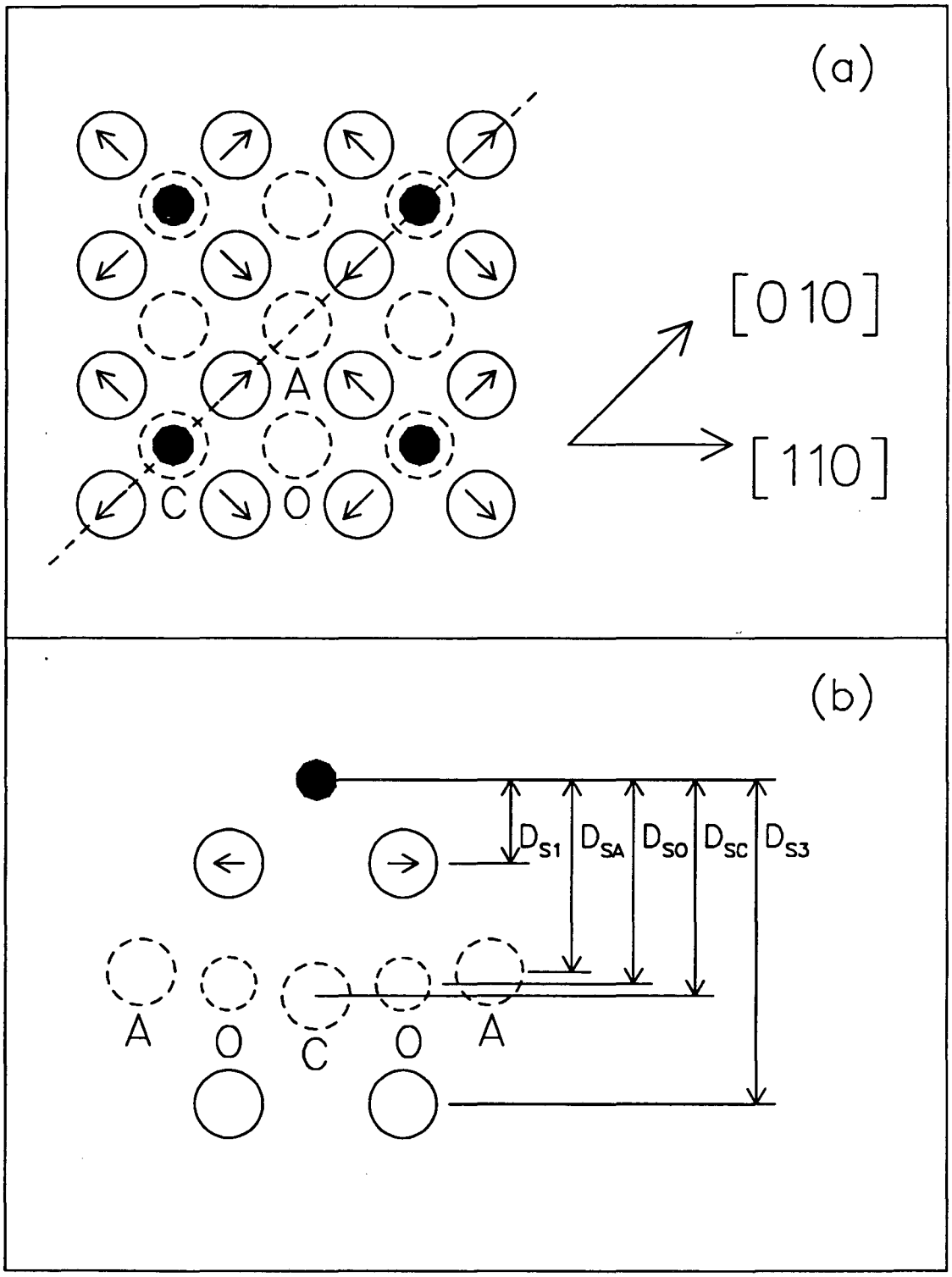

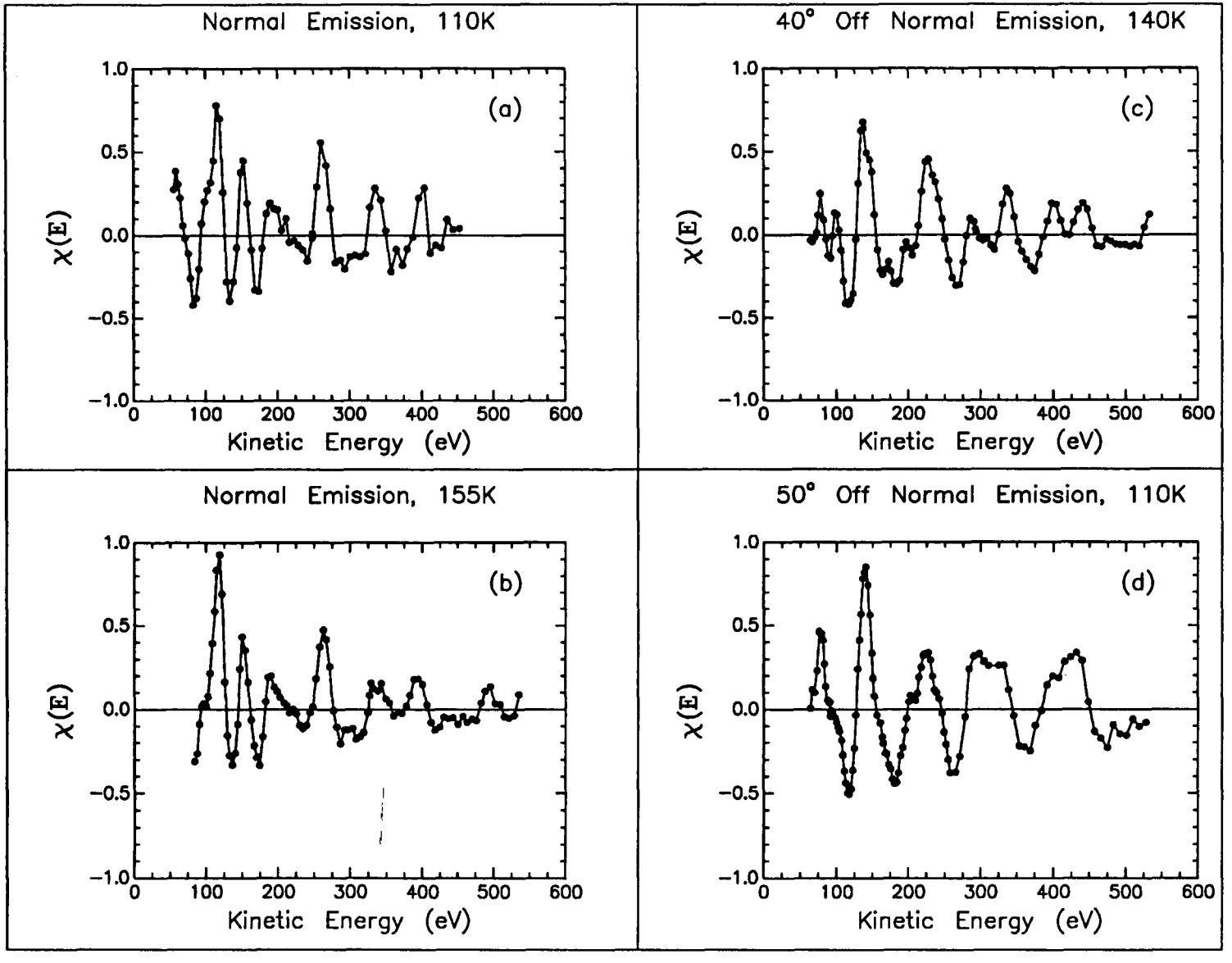


Figure: 3: p(2×2)S/Cu(001) Raw Data.

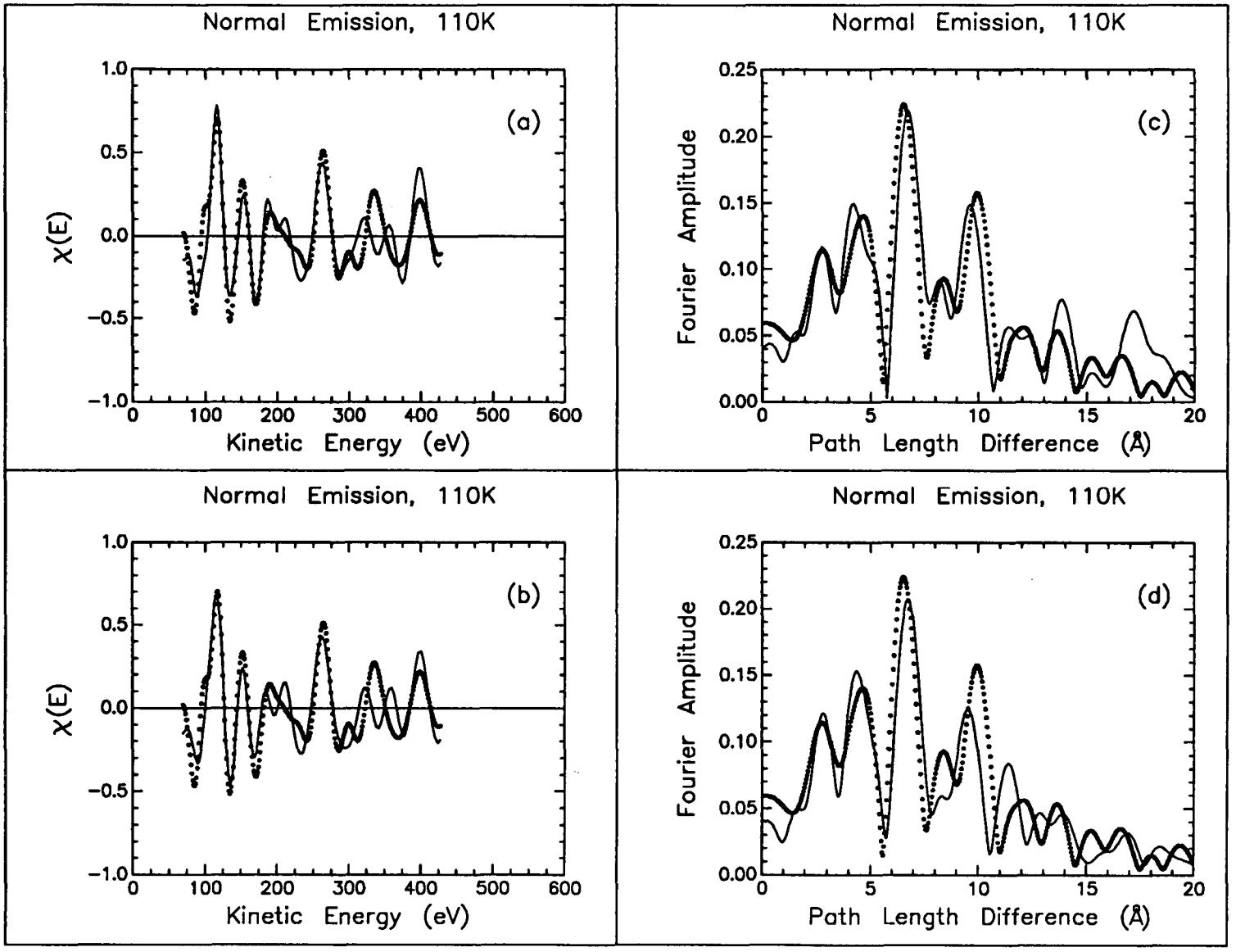


Figure: 4: Fits to 110 K Normal Emission Data, p(2×2)S/Cu(001).

Figure: 5: Fits to 155 K Normal Emission Data, p(2×2)S/Cu(001).

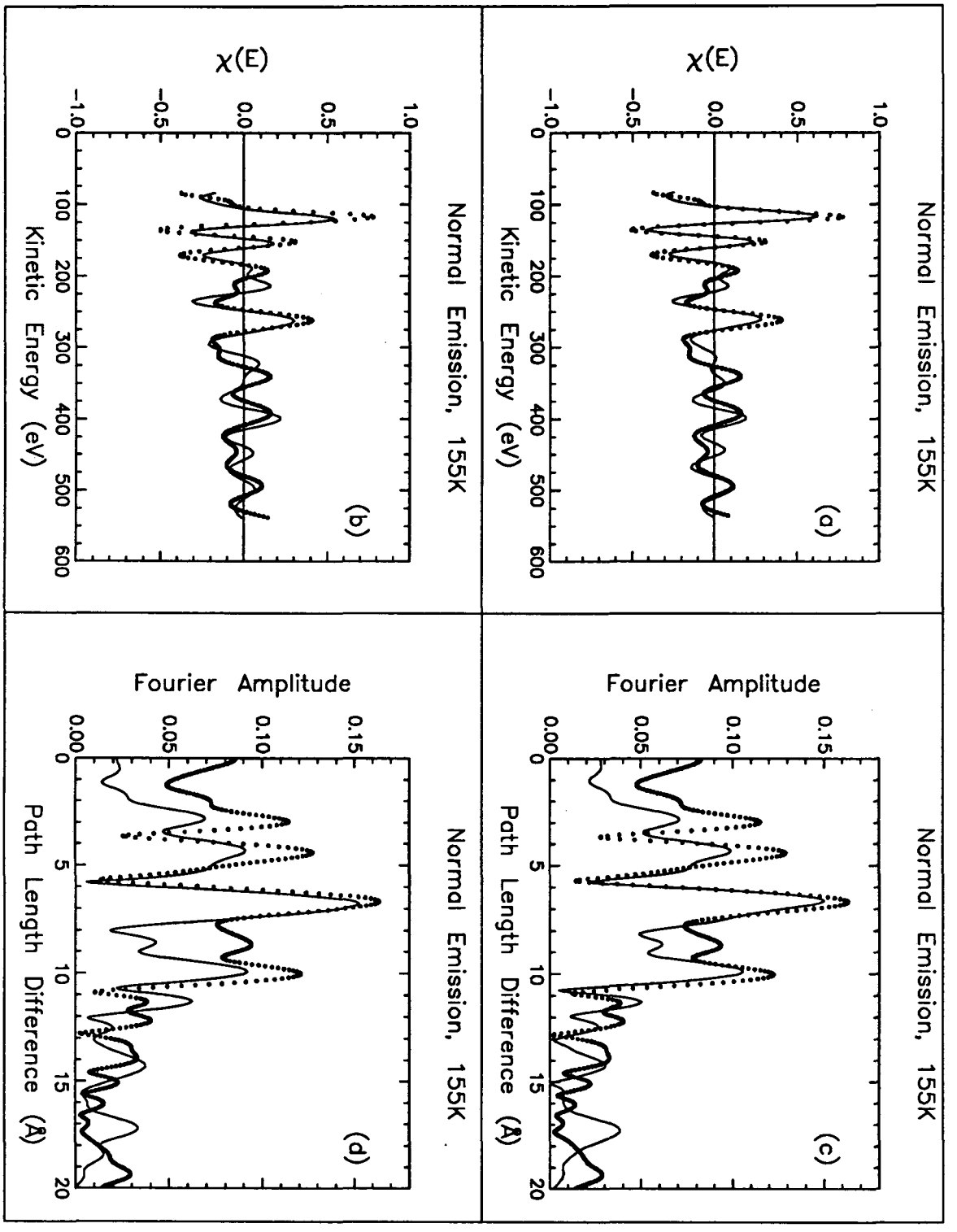

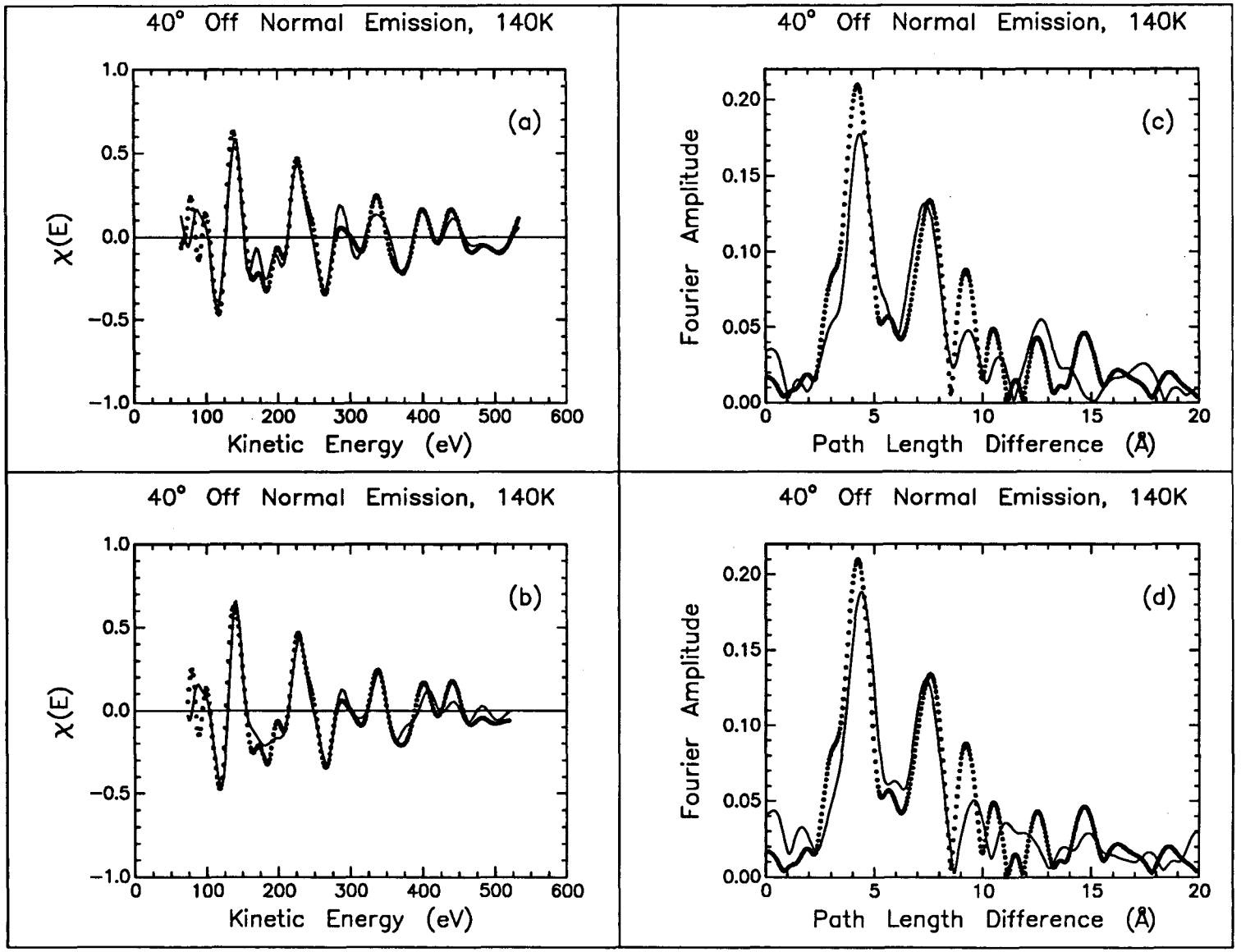


Figure: 6: Fits to 40° Off Normal Emission Data, p(2×2)S/Cu(001).

Figure: 7: Fits to 50° Off Normal Emission Data, p(2×2)S/Cu(001).

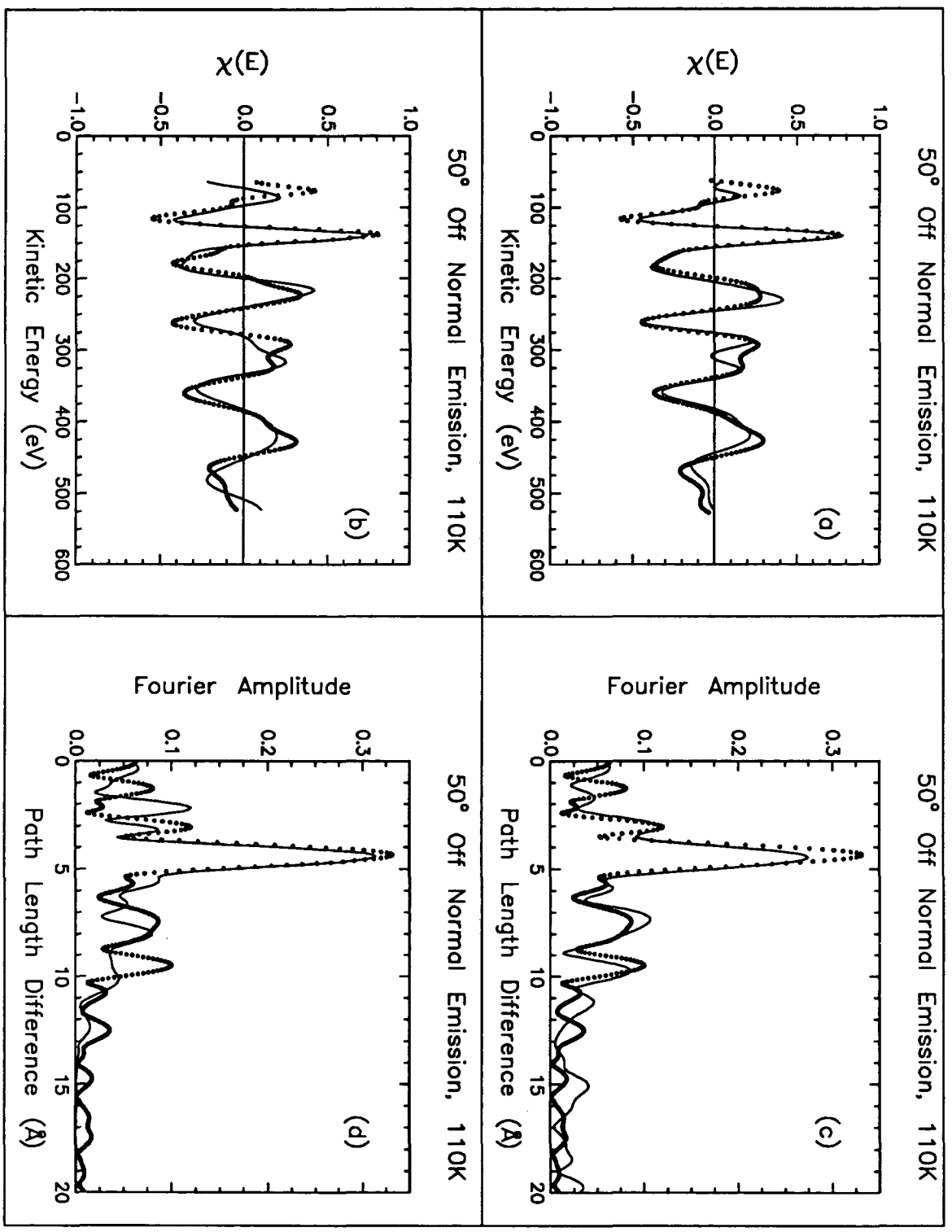

Figure: 8: R-Factors vs. Second Cu Layer Displacements, p(2×2)S/Cu(001).

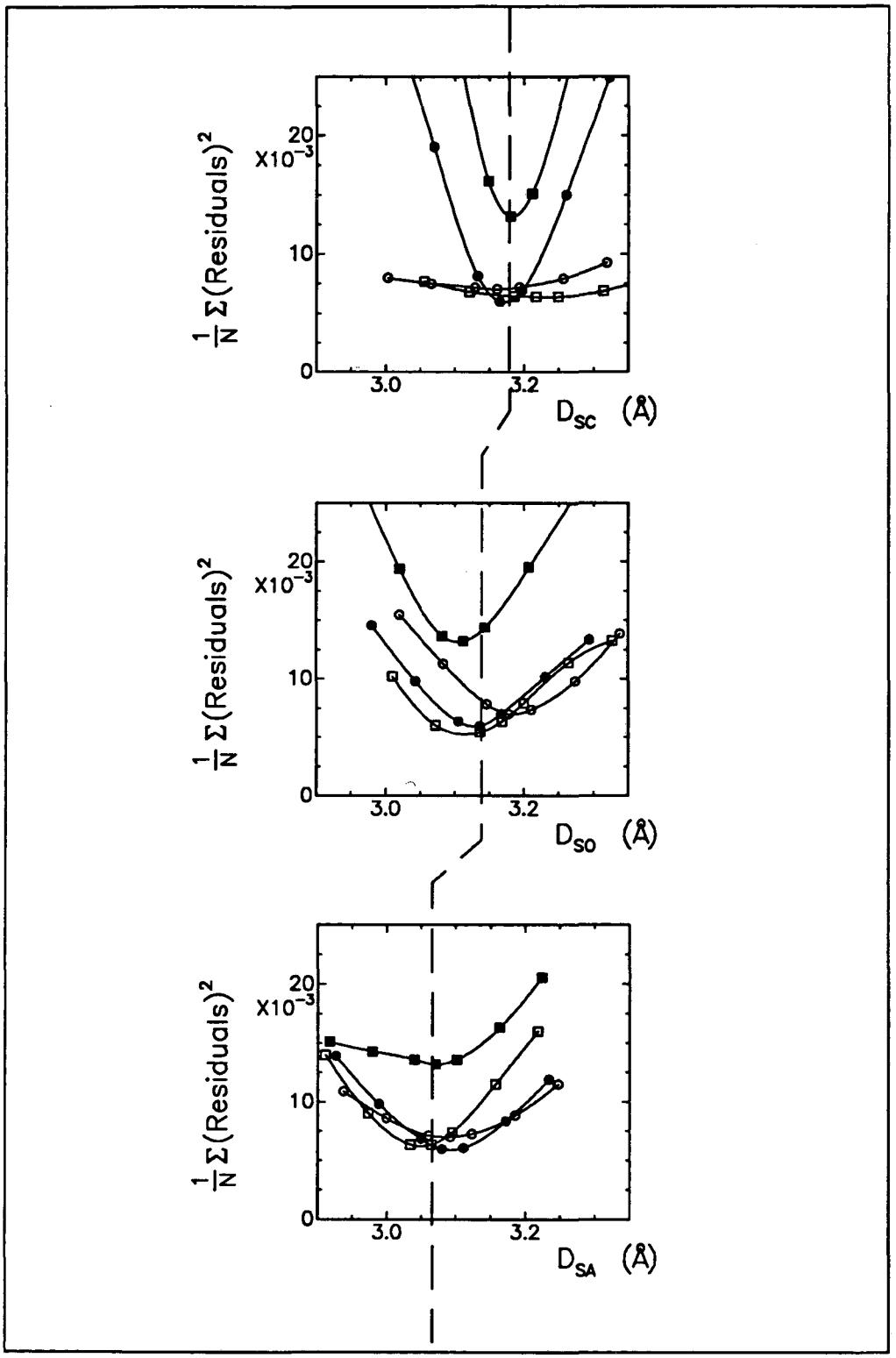

Figure: 9: Effect of Temperature on $\chi$ Oscillations, p(2×2)S/Cu(001).

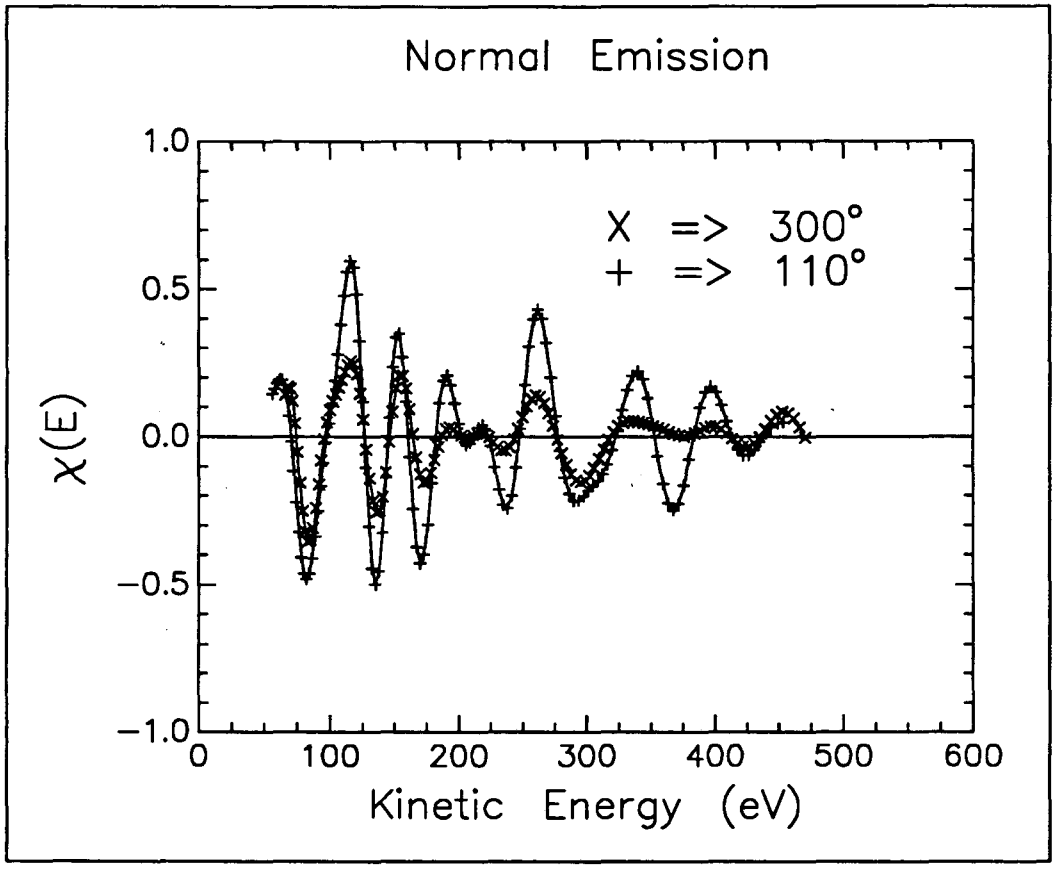

Figure: 10: Refit of 300 K Normal Emission Data, p(2×2)S/Cu(001).

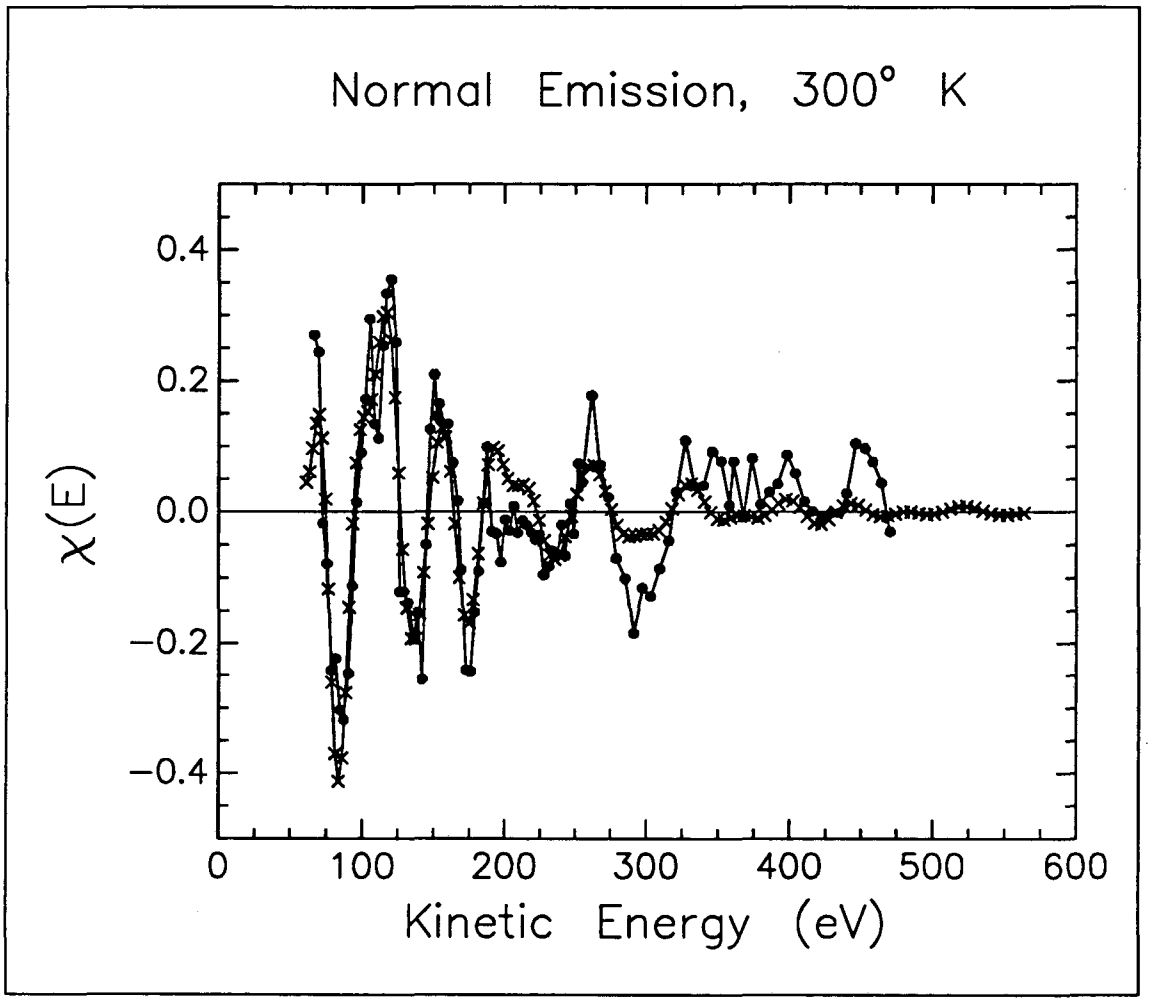

LAWRENCE BERKELEY LABORATORY
UNIVERSITY OF CALIFORNIA
INFORMATION RESOURCES DEPARTMENT
BERKELEY, CALIFORNIA 94720